Supporting info

Table S1 Optimized synthesis conditions of the MOF-coatings

	Cu(CHDA)	$Cu_3(BTC)_2$	$Cu(INA)_2$
Time (Sec.)	15	180	60
Voltage (V)	30	2.5	2.5
Frequency (Hz)	0.5	0	0
Solvent (ml) EtOH : H_2O	75 : 25	50 : 50	50 : 50

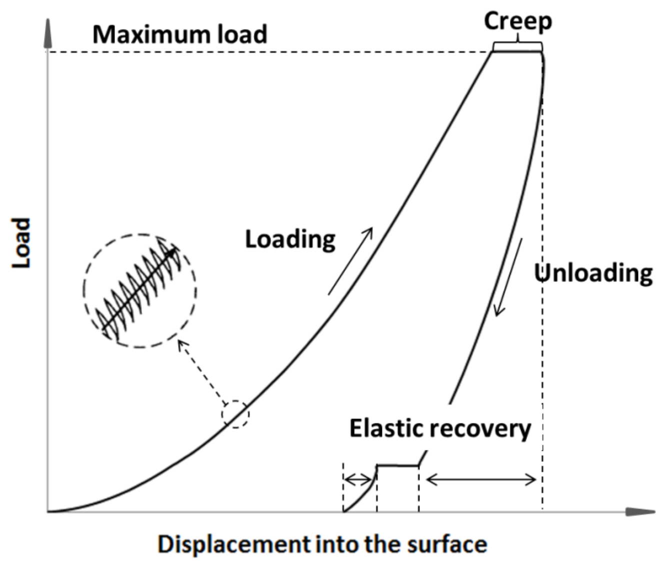

Figure S1. A typical load-displacement curve. On the unloading curve, the horizontal segment at 90% unload corresponds to thermal drift measurement.

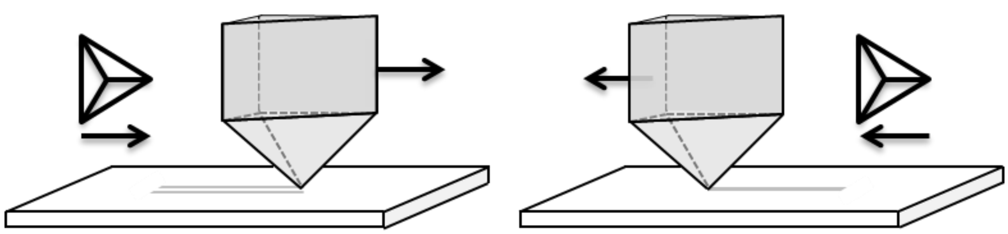

Figure S2 The scratch movements depending on the geometry of the indenter, with either the sharp tip (left, denoted as 0°) or blunt side (right, at 180°) facing ~~in~~ the scratching direction.

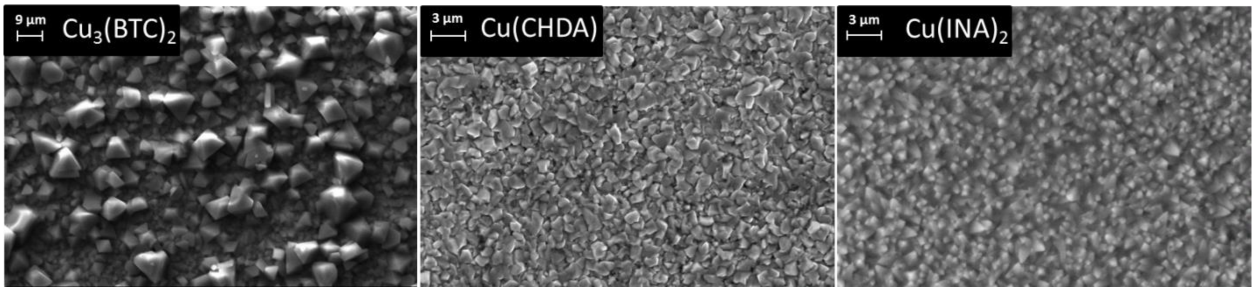

Figure S3 Details of the electrochemical growth of $Cu_3(BTC)_2$, Cu(CHDA) and $Cu(INA)_2$ on copper anodes.

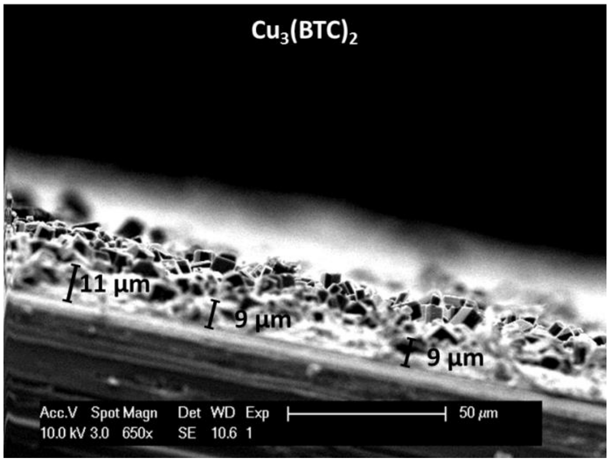

Figure S4 Cross-section SEM of the $Cu_3(BTC)_2$ coating on a copper anode, with a thickness of 9-11 µm

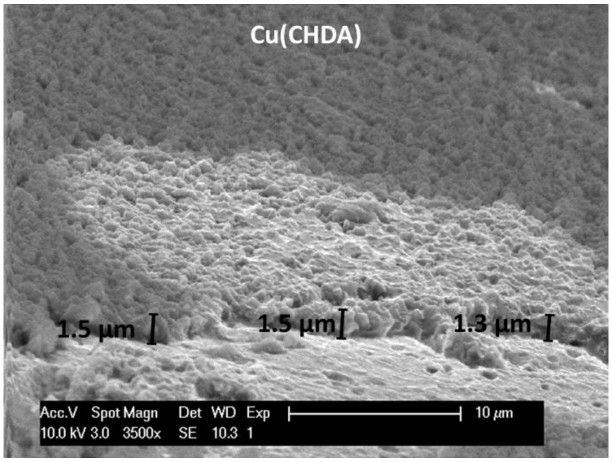

Figure S5 Cross-section SEM of the Cu(CHDA) coating on a copper anode, with a thickness of 1.3-1.5 µm.

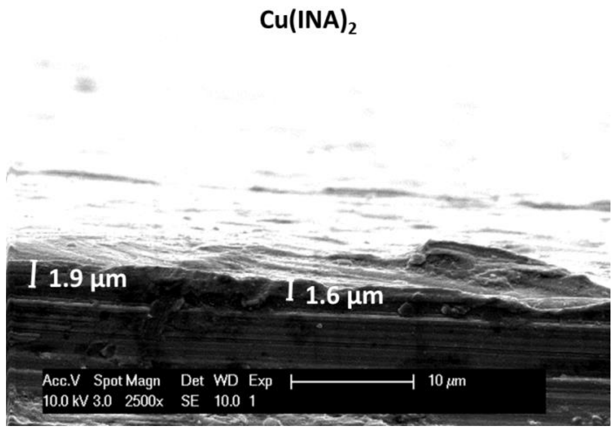

Figure S6 Cross-section SEM of the Cu(INA)$_2$ coating on a copper anode, with a thickness of 1.6-1.9 µm.

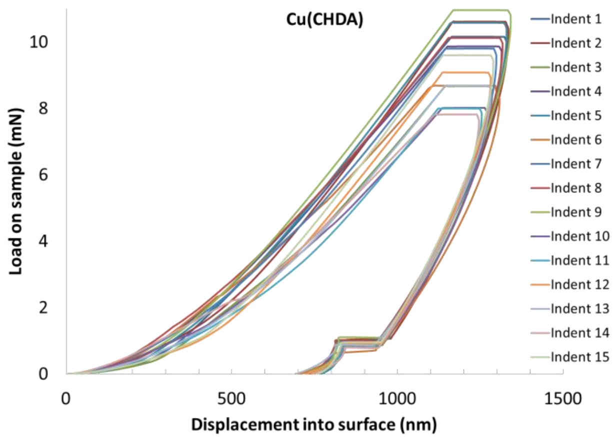

Figure S7 Load-displacement curves of 15 indents on Cu(CHDA).

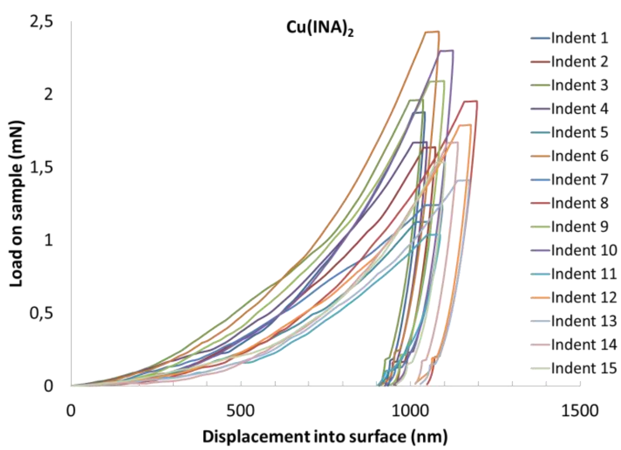

Figure S8 Load-displacement curves of 15 indents on Cu(INA)$_2$.

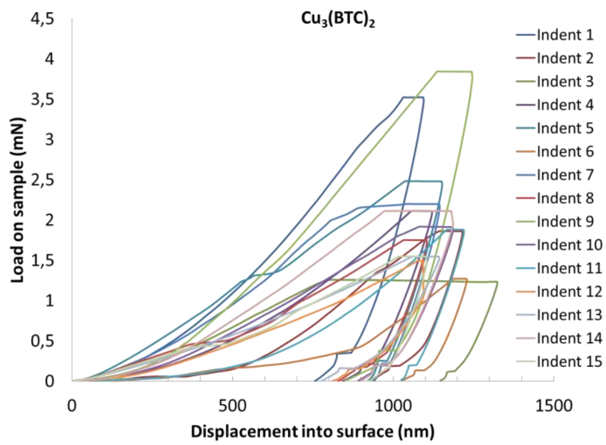

Figure S9 Load-displacement curves of 15 indents on $Cu_3(BTC)_2$.

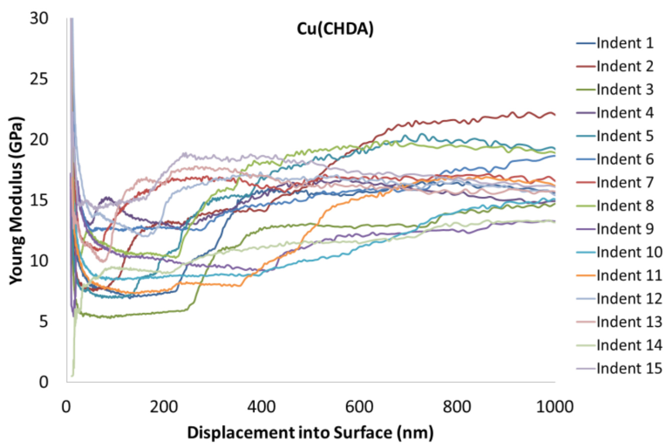

Figure S10 Young's moduli as a function of indentation depth for 15 indents on Cu(CHDA).

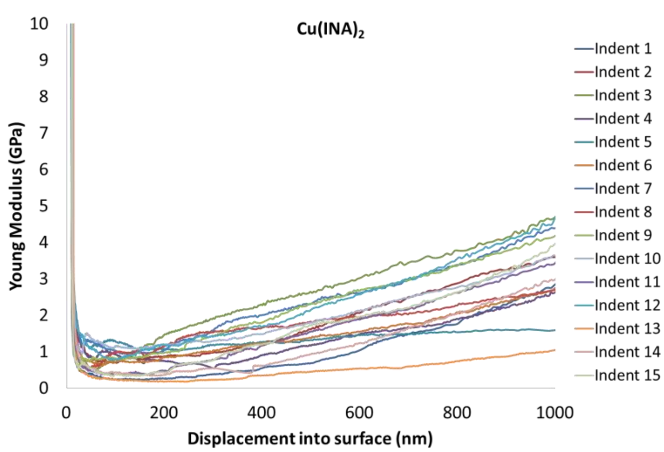

Figure S11 Young's moduli as a function of indentation depth for 15 indents on $Cu(INA)_2$.

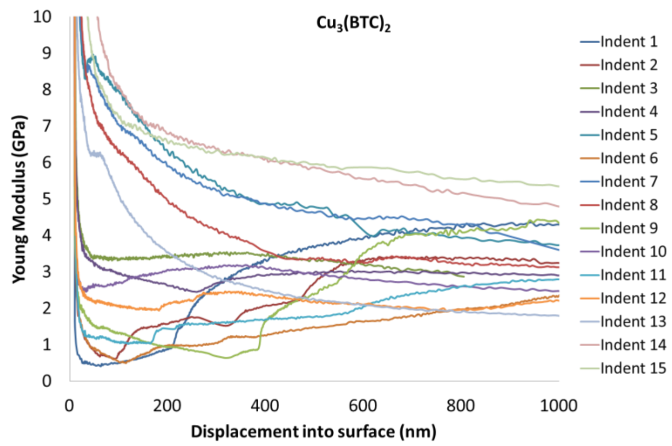

Figure S12 Young's moduli as a function of indentation depth for 15 indents on $Cu_3(BTC)_2$.

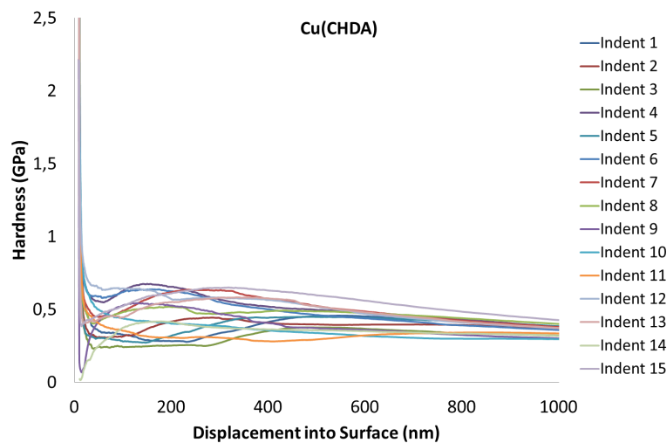

Figure S13 Hardness as a function of indentation depth for 15 indents on Cu(CHDA).

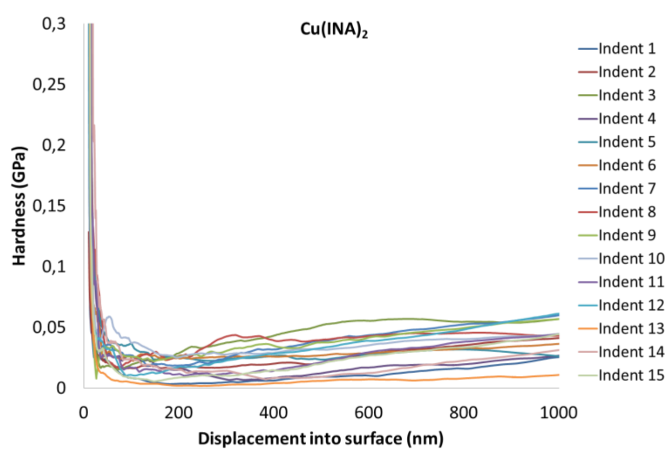

Figure S14 Hardness as a function of indentation depth for 15 indents on $Cu(INA)_2$.

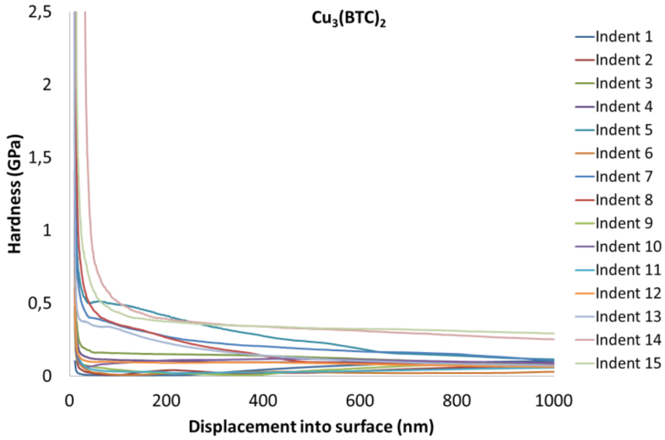

Figure S15 Hardness as a function of indentation depth for 15 indents on $Cu_3(BTC)_2$.

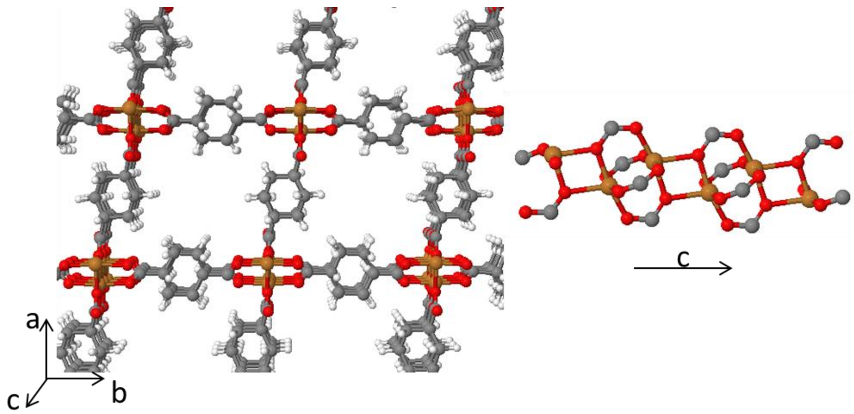

Figure S16 The structure of Cu(*trans*-1,4-cyclohexanedicarboxylate) with the 1D pores (left), the inorganic Cu-oxo-chain forming the rigid pillar of the structure in the *c*-direction (right).

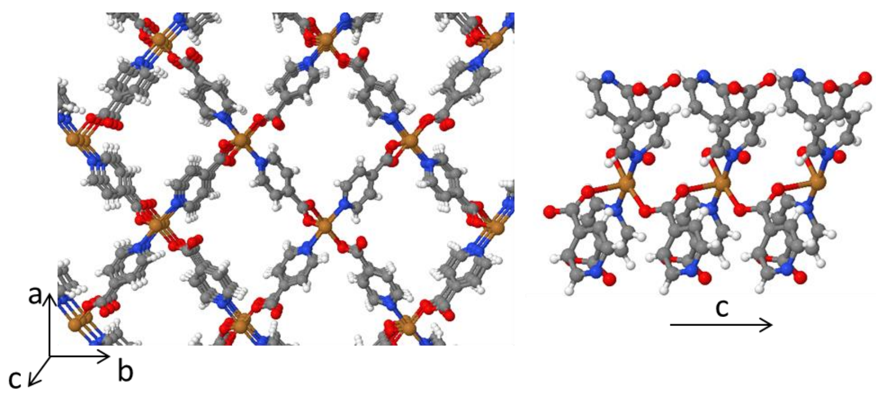

Figure S17 The structure of $Cu(isonicotinate)_2$ with the 1D pores (left), square pyramidal copper atoms coordinated by two pyridyl groups and two carboxylate groups of four isonicotinate units in a monodentate fashion at the equatorial positions, together with one carboxylate of an isonicotinate in apical position (right).

This journal is © The Royal Society of Chemistry 2013

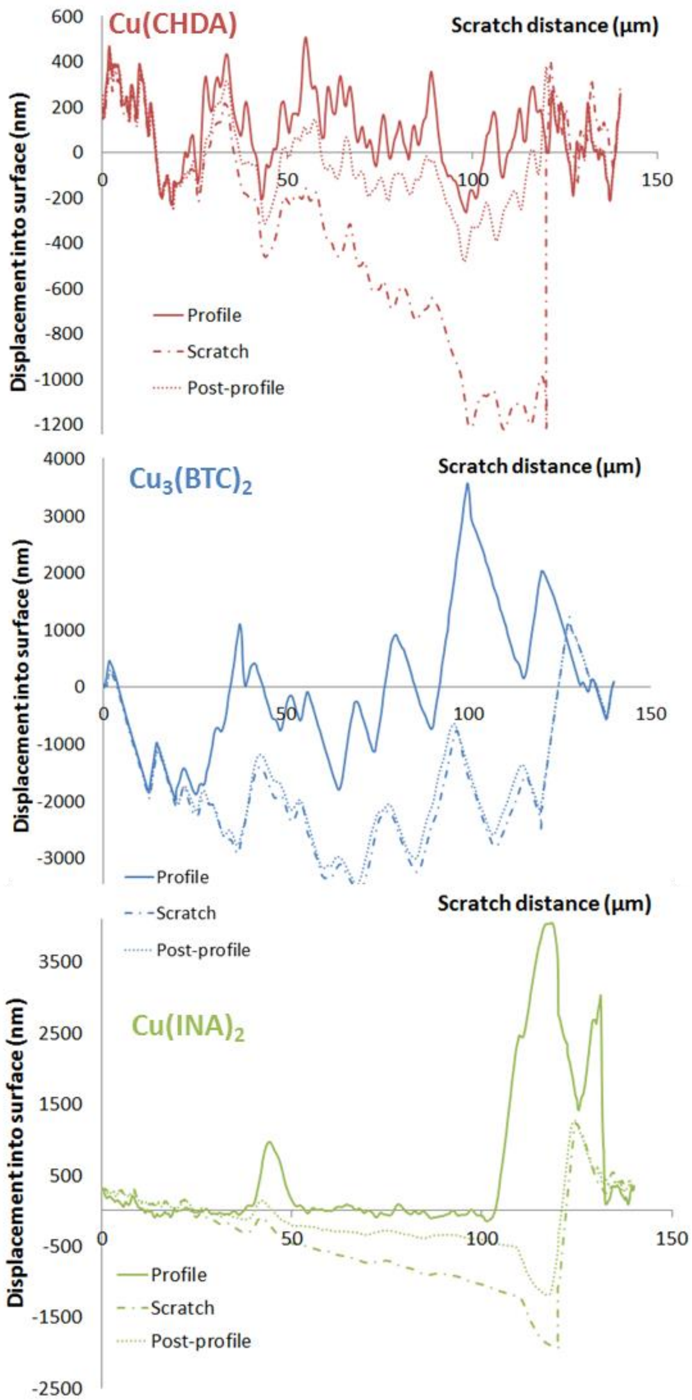

Figure S18. Scratch profiles in the push mode with the displacement into the surface as a function of scratch distance. The load was set at 0 mN at 20μm and linearly increased up to 10 mN at 120 μm

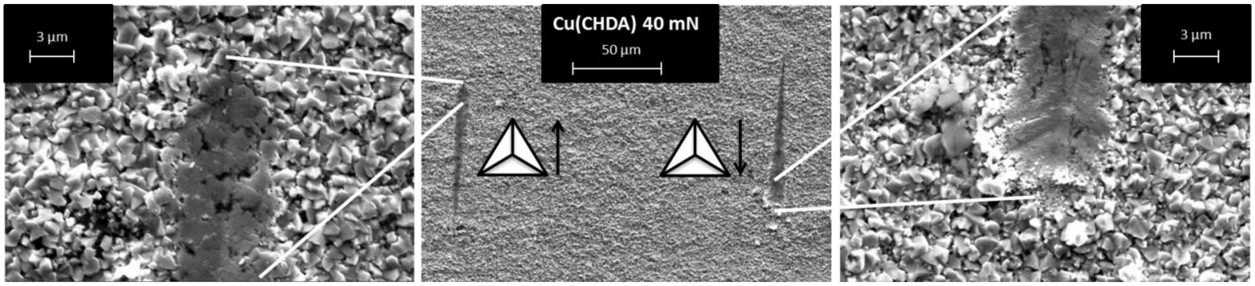

Figure S19. Scratch profiles of Cu(CHDA) with a maximum load of 40mN; the side panels show details of the residual scratch.

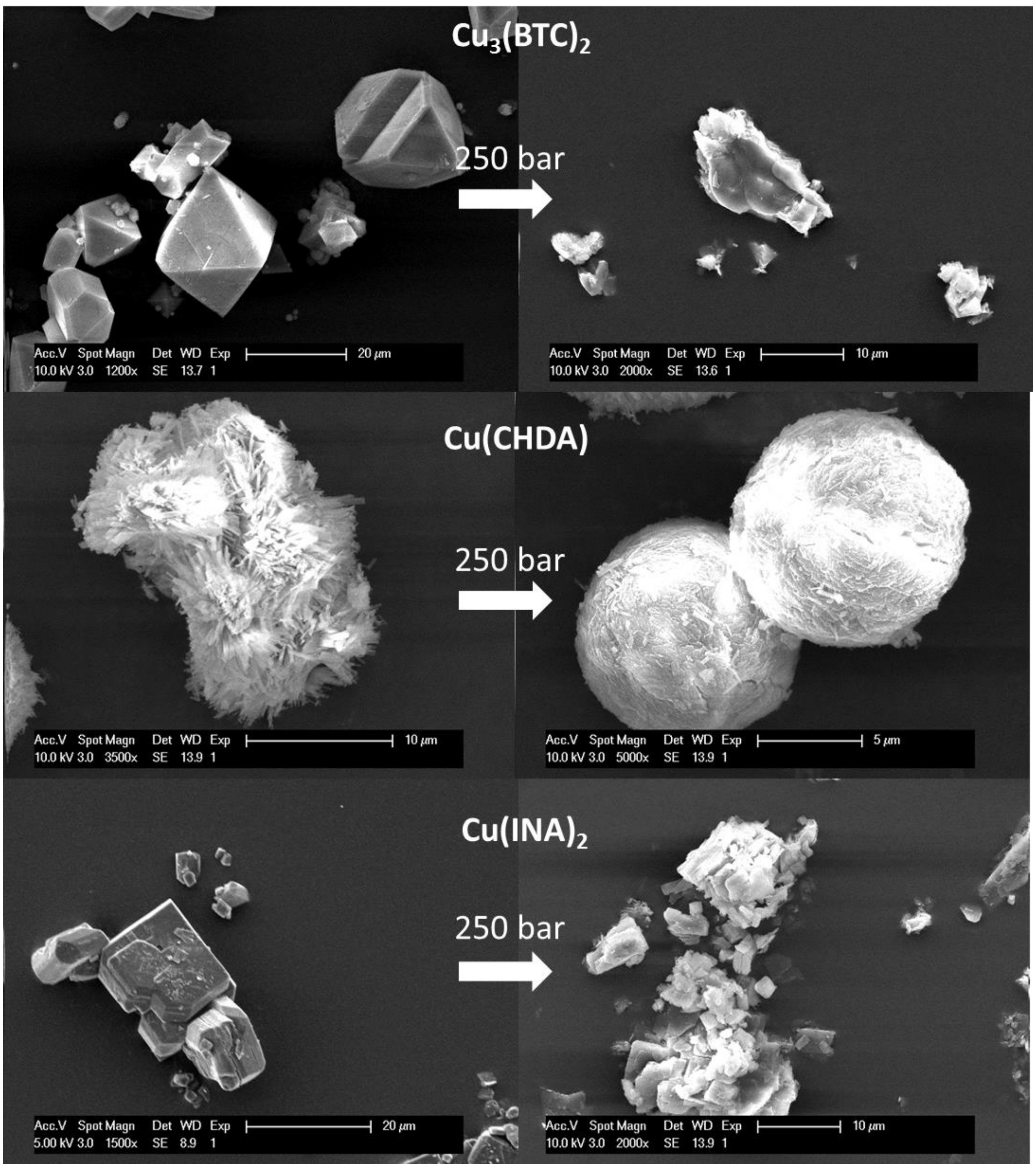

Figure S20. SEM pictures of solvothermally synthesised $Cu_3(BTC)_2$, Cu(CHDA) and $Cu(INA)_2$; before and after 250 bar uniaxial pressure.

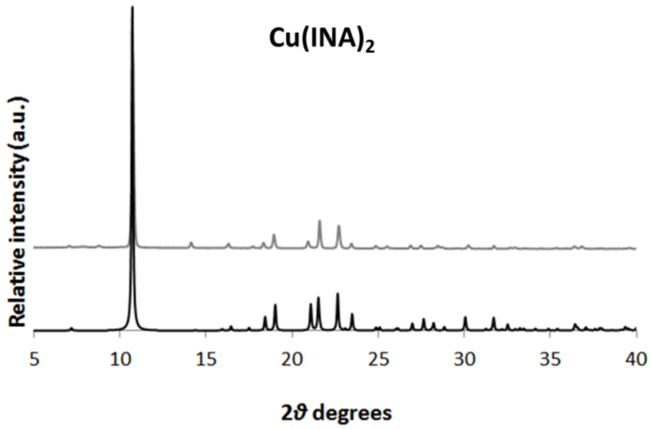

Figure S21. Thin film XRD pattern of $Cu(INA)_2$ collected from a film grown on a pure copper electrode (top) and reference XRD pattern (bottom).

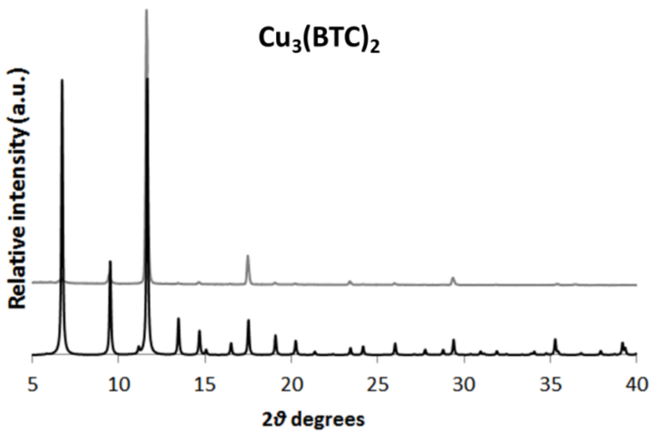

Figure S22. Thin film XRD pattern of $Cu_3(BTC)_2$ collected from a film grown on a pure copper electrode (top) and reference XRD pattern (bottom).

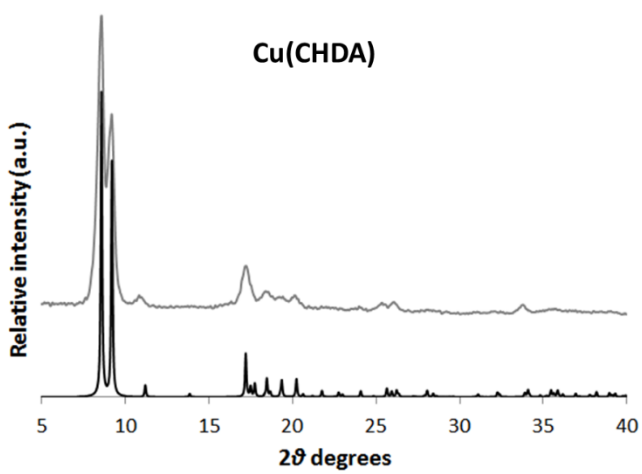

Figure S23. Thin film XRD pattern of Cu(CHDA) collected from a film grown on a pure copper electrode (top) and reference XRD pattern (bottom).

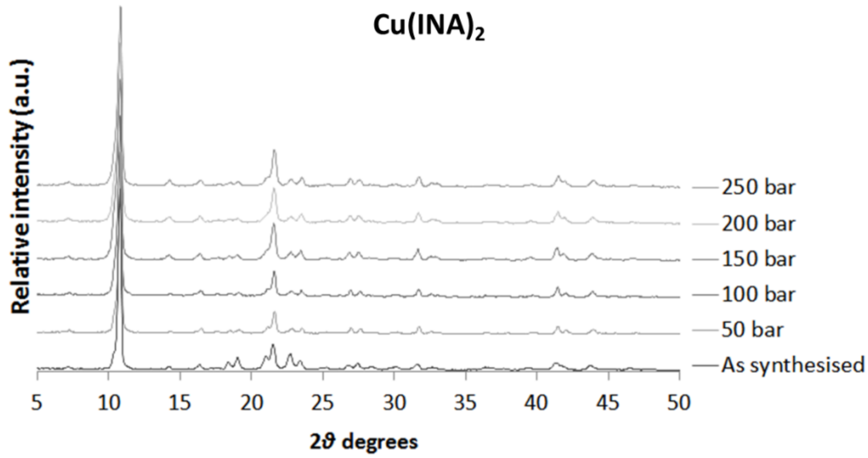

Figure S24. XRD patterns of Cu(INA)$_2$ powders before (as synthesised) and after certain applied pressures (X bar).

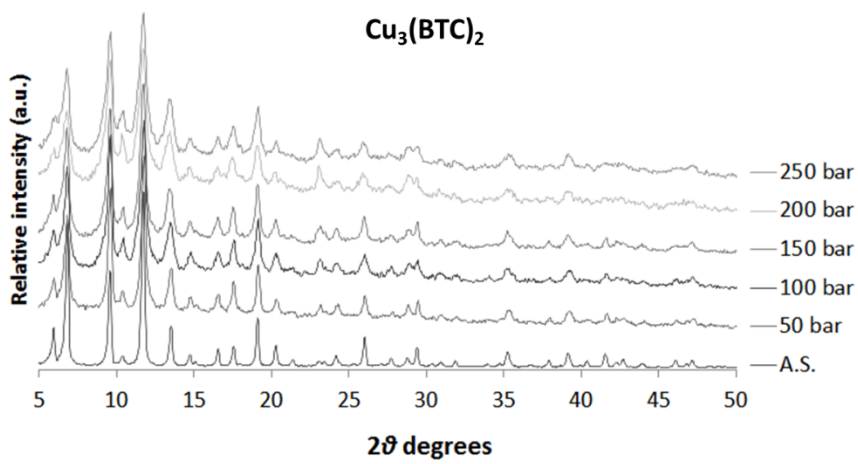

Figure S25. XRD patterns of Cu$_3$(BTC)$_2$ powders before (as synthesised) and after certain applied pressures (X bar).

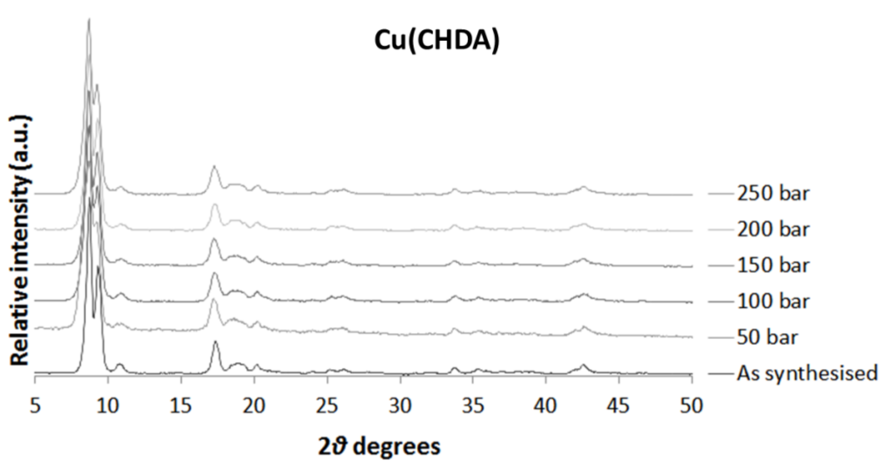

Figure S26. XRD patterns of Cu(CHDA) powders before (as synthesised) and after certain applied pressures (X bar).